remote sensing

MDPI

Letter

Daily Variation of Chlorophyll-A Concentration Increased by Typhoon Activity

Suginori Iwasaki

Department of Earth and Ocean Sciences, National Defense Academy of Japan, 1-10-20 Hashirimizu, Yokosuka, Kanagawa 239-8686, Japan; iwasaki@nda.ac.jp

Received: 17 March 2020; Accepted: 15 April 2020; Published: 16 April 2020

check for updates

Abstract: The chlorophyll-a (Chla) concentration product of the Himawari-8 geostationary meteorological satellite is used to show the temporal variation of Chla owing to the passage of typhoons, namely, tropical cyclones in the western North Pacific Ocean. The daily Chla variation shows that Chla usually increases along the paths of typhoons, whereas the same observations are almost impossible when using the data of polar-orbiting satellites as shown in previous studies. This is because the temporal resolution of Himawari-8 is ten times more than that of polar-orbiting satellites, and the daily Chla distribution contains a few disturbances attributed to clouds after compositing cloud-free data. Chla usually increases on the day of typhoon arrival, but mostly, the ratio of Chla increased by a typhoon to the background Chla, $R_{\mathrm{Chla}}^{\mathrm{HIMA}}$, is less than 2. Only a few typhoons considerably increased Chla. As a whole, $R_{\mathrm{Chla}}^{\mathrm{HIMA}}$ is proportional to the maximum 10-min sustained wind speed up to 85 knots (44 m s^{-1}), namely, 0.01 mg m^{-3} $knot^{-1}$ (0.019 mg s m^{-4}). However, there is no clear dependence between Chla and the wind speed in seas with higher Chla, such as the South China Sea. The result that typhoons are usually cultivating the ocean is important for studies of primary ocean productivity and carbon flux between the atmosphere and ocean.

Keywords: phytoplankton bloom; enhancement of chlorophyll-a concentration; tropical cyclone; Himawari-8; daily variation

1. Introduction

As the primary product of the ocean, phytoplankton is important for ecosystems [1] and carbon cycles [2]. Typhoons, namely tropical cyclones in the North Pacific Ocean, sometimes induce phytoplankton blooms because of upwelling and vertical mixing. For example, Shih et al. [3] performed ship-borne measurements of chlorophyll-a (Chla) concentrations and particulate organic carbon flux (POC) a week before and 4–7 days after Typhoon Jangmi passed. They showed that Chla and POC were enhanced after the typhoon passed. However, because in situ measurements around a typhoon are dangerous, following research used space-borne data to estimate Chla. Lin et al. [4] showed that typhoon Kai-Tak increased Chla in the South China Sea to a level that was 30 times greater than that before Kai-Tak passed. Chen and Tang [5] showed that the category-1 typhoon Linfa induced an eddy feature Chla bloom that lasted for 17 days. Lin [6] showed that two of 11 typhoons in 2003 increased Chla, although not the super-typhoon Maemi, whose maximum 1-min sustained wind speed was 150 knots (77 m s^{-1}). Those studies used observational data from instruments on polar-orbiting satellites, such as the Moderate Resolution Imaging Spectroradiometer (MODIS) and the Sea-Viewing Wide Field-of-View Sensor (SeaWiFS), to measure the Chla increase due to typhoons. However, because polar-orbiting satellites have relatively low temporal resolution, namely once every few days, Lin [6] used weekly Chla data, which are not suitable for measuring the daily variation of Chla distributions.

Launched in 2010, the Geostationary Ocean Color Imager (GOCI) is the first geostationary satellite that can measure ocean colors [7]. Because the temporal resolution of GOCI is 1 h, He et al. [8], for example, were able to use GOCI to show that a typhoon in a coastal area increased the total suspended particle matter for a duration of less than a day. GOCI retrieves Chla with less cloud disturbance than MODIS and SeaWiFS do. This is because even if Chla retrieval at a given moment is impossible because of cloudiness, the daily Chla can still be retrieved at another time on the same day when there is no cloud. Therefore, the daily Chla retrieved by GOCI suffers from less lack of data than that obtained by polar-orbiting satellites when compositing with cloud-free data. However, GOCI is not suitable for measuring the increase in Chla by all typhoons because the observational area of GOCI is the ocean around the Korean Peninsula, and the southern limit of GOCI measurements is close to 25°N (e.g., Figure 1 of Ryu et al. [7]).

Launched in 2014, the Himawari-8 geostationary meteorological satellite can retrieve Chla since July 2015 [9]. Its temporal resolutions are 10 min in the hemisphere, whose center is 140.7°E, and 2.5 min around Japan. That is, Himawari-8, unlike GOCI, can be used to measure the tropical regions where many typhoons occurred. Himawari-8 also has six times (24 times) more chances to measure cloud-free data than GOCI in the subtropics (around Japan). Therefore, Himawari-8 is more suitable than GOCI for measuring the increase in the Chla owing to typhoons. Shen et al. [10] used GOCI and Himawari-8 to retrieve Chla and presented a case study of the category-4 typhoon Malakas, which increased Chla and decreased sea surface temperature (SST) where it passed the northern sea of Taiwan.

This study focuses on retrieving the daily variation of Chla owing to typhoons, such as by applying statistical analysis to 4-year data to establish how the Chla increase is related to typhoon wind speed and ocean area. Since the daily variation of Chla was hardly measured by sensors on polar-orbiting satellites, the relationship between a typhoon and a phytoplankton bloom is not well known. This study also examines the daily variation of SST because the SST retrieved by Himawari-8 has better temporal and spatial resolutions than that retrieved by polar-orbiting microwave imagers such as the Advanced Microwave Scanning Radiometer 2 (AMSR-2) [11].

2. Data

The typhoon parameters that are used are those estimated by the Japan Meteorological Agency (JMA), including the lowest pressure, the maximum 10-min sustained wind speed, and the latitude and longitude of the center of each typhoon. These parameters are reported usually every 6 h (3, 9, 15, and 21 UTC) but more often when a typhoon is near Japan. The parameters at 6 UTC, 15 in local time at a longitude of 135°E, are used because we seek to analyze daytime Chla. The wind speed of typhoons of the Japan Meteorological Agency (JMA) use knot; hence, wind speed has been provided in the units of knots and m s^{-1} in this study.

Figure 1 shows the occurrence numbers and wind speed distribution of typhoons between August 2015 and July 2019. In those four years, 103 typhoons occurred, the majority (87, 84%) between July and November (Figure 1a). The greatest maximum 10-min sustained wind speed of the typhoons was 120 knots (62 m s^{-1}), and the mode of the 10-min maximum wind speed occurrence was 35–40 knots (18–21 m s^{-1}; Figure 1b). Typhoons were present on 519 days in total (the sum of "number of days" in Figure 1b), thus their average lifetime was 5 days. Typhoons tend to exist at longitudes of 145° or less and at latitudes between 10° and 35° (not shown).

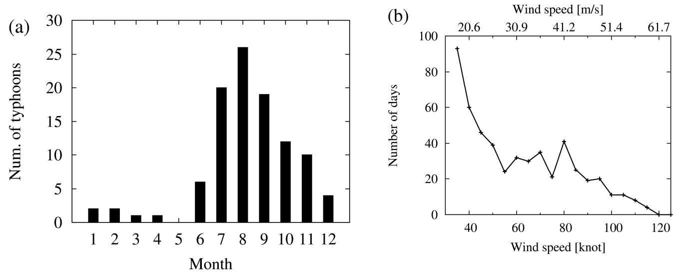

Figure 1. (**a**) Occurrence number of typhoons between August 2015 and July 2019. (**b**) Occurrence of maximum 10-min sustained wind speed of each typhoon at 6 UTC each day.

Two types of Chla data sets are used. One is Chla retrieved by the Himawari-8 geostationary meteorological satellite [12], provided by the P-tree system of Japan Aerospace Exploration Agency (JAXA), and another is Chla retrieved by the MODIS on board the Aqua satellite in a near-polar low Earth orbit, provided by the Ocean Biology Processing Group of the Ocean Ecology Laboratory of the NASA Goddard Space Flight Center [13]. Himawari-8 and MODIS retrieve Chla by using the empirical function of the reflectivities of the visible bands, thus Chla is retrievable in daytime on clear days. Murakami [12] has shown that Chla of Himawari-8 becomes noisy at 35° or higher latitude of the winter hemisphere owing to the long path of the solar light. This noise does not affect this research because most typhoons occur between July and November (Figure 1a) at 35° or lower latitude.

The temporal resolutions of Himawari-8 and MODIS are 10 min and once every few days, respectively. The horizontal distribution of Chla retrieved by Himawari-8 has less lack of data than that by MODIS in the western North Pacific, because Himawari-8 has ten times more chances to retrieve Chla than MODIS does. The horizontal resolution of the Chla products of Himawari-8 and MODIS are 0.05° (approx. 5 km) and approximately 0.04° (approx. 4 km), respectively.

This study used the daily Chla for our analysis and the monthly Chla to remove the striping noise of the Himawari-8 Chla as described in the Appendix A. $\mathrm{Chla}^{\mathrm{HIMA}}$ denotes the Himawari-8 Chla with noise removed (see Appendix A) and $\mathrm{Chla}^{\mathrm{MODIS}}$ denotes the MODIS Chla.

This study also used the daily data of skin and subskin SSTs retrieved respectively by Himawari-8 ($\mathrm{SST}^{\mathrm{HIMA}}$; [14]) and AMSR-2 ($\mathrm{SST}^{\mathrm{AMSR2}}$; [11]) on board the Global Change Observation Mission-W1 (GCOM-W1) that is in a sun-synchronous orbit. $\mathrm{SST}^{\mathrm{HIMA}}$ and $\mathrm{SST}^{\mathrm{AMSR2}}$ are provided by the P-Tree system and the G-Portal system of JAXA, respectively. $\mathrm{SST}^{\mathrm{HIMA}}$ and $\mathrm{SST}^{\mathrm{AMSR2}}$ are retrieved from the thermal emission at depths of less than 500 μm and 1 mm, respectively. For a conceptual diagram of skin and subskin SSTs, see Figure 1 of Donlon et al. [15]. The temporal and horizontal resolutions of AMSR-2 are once every few days and 35 × 62 km at a frequency of 6.9 GHz, respectively, where the vertical polarization of 6.9 GHz is used for SST retrieval. The horizontal resolutions of the $\mathrm{SST}^{\mathrm{HIMA}}$ and $\mathrm{SST}^{\mathrm{AMSR2}}$ products that I used are 0.02° (approx. 2 km) and 0.1° (approx. 10 km), respectively. $\mathrm{SST}^{\mathrm{HIMA}}$ is retrievable in the daytime on clear days, whereas $\mathrm{SST}^{\mathrm{AMSR2}}$ is retrievable even at cloudy nighttime. $\mathrm{SST}^{\mathrm{AMSR2}}$ is not retrievable in rainfall.

To compare Chla and SST at the same place, the rates of Chla increase (Equation (1a,b)) and SST decrease (Equation (2a,b)) were introduced, namely:

$$\mathrm{R}_{\mathrm{Chla}}^{\mathrm{HIMA}} = \mathrm{Chla}^{\mathrm{HIMA}} / \mathrm{Chla}_{\mathrm{3d\ before}}^{\mathrm{HIMA}} \tag{1a}$$

$$\mathrm{R}_{\mathrm{Chla}}^{\mathrm{MODIS}} = \mathrm{Chla}^{\mathrm{MODIS}} / \mathrm{Chla}_{\mathrm{3d\ before}}^{\mathrm{MODIS}} \tag{1b}$$

$$\delta\mathrm{SST}^{\mathrm{HIMA}} = \mathrm{SST}^{\mathrm{HIMA}} - \mathrm{SST}_{\mathrm{3d\ before}}^{\mathrm{HIMA}} \tag{2a}$$

$$\delta\mathrm{SST}^{\mathrm{AMSR2}} = \mathrm{SST}^{\mathrm{AMSR2}} - \mathrm{SST}_{\mathrm{3d\ before}}^{\mathrm{AMSR2}} \tag{2b}$$

The parameters within a bracket (e.g., $\langle \mathrm{Chla}^{\mathrm{HIMA}} \rangle$) denote the medians of the parameters (e.g., $\mathrm{Chla}^{\mathrm{HIMA}}$) within 100 km from the daily center at each point along the typhoon trajectory. This study uses medians instead of averages because a few outliers sometimes considerably change the average. The parameters with a subscript "3d before" (e.g., $\mathrm{Chla}_{\mathrm{3d\ before}}^{\mathrm{HIMA}}$) are the same as the parameters without the subscript (e.g., $\mathrm{Chla}^{\mathrm{HIMA}}$) but for three days before. The parameters with a subscript "3d before" are assumed as the background values of Chla and SST.

3. Results

Figure 2 shows examples of the $\mathrm{Chla}^{\mathrm{HIMA}}$, $\mathrm{Chla}^{\mathrm{MODIS}}$, $\mathrm{SST}^{\mathrm{HIMA}}$, and $\mathrm{SST}^{\mathrm{AMSR2}}$ distributions of Typhoon Yutu, whose minimum pressure and maximum 10-min sustained wind speed on 24–30 October, 2018 were 915–985 hPa and 55–105 knots (26–54 m s^{-1}), respectively. Figure 2(a4–a7) show that $\mathrm{Chla}^{\mathrm{HIMA}}$ increased after the typhoon passed at 18°N and 125°E–140°E. Figure 2(b7) also shows that $\mathrm{Chla}^{\mathrm{MOIDIS}}$ increased at 18°N and 130°E; however, the $\mathrm{Chla}^{\mathrm{MODIS}}$ time sequence is not clear as few data were retrieved because of cloudiness and lack of observations. Figure 2(c4–c7) show that SST^{HIMA} decreased along the path of the typhoon. SST^{AMSR2} also decreased along the path, around 18°N and 130°E (Figure 2(d6,d7)). SST^{HIMA} is also clearer than SST^{AMSR2} because the observation frequency and horizontal resolutions of AMSR-2 are sparser and coarser than those of Himawari-8. The typhoon in late October was chosen in Figure 2 to avoid unclear Chla and SST tendencies because some Chla and SST horizontal distributions from July to September have tracks of Chla increases and SST decreases induced by previous typhoons. The tendencies of the Chla increases and the SST decreases are almost common for all typhoons, but those on day 0 (the day of typhoon arrival) are sometimes unclear because of lack of data due to cloudiness. Figure 2 shows that Himawari-8 has the potential to retrieve daily variations of Chla and SST distributions.

The lowest pressure and the greatest maximum 10-min sustained wind speed were 900 hPa and 115 knots (59 m s^{-1}), respectively, around 15°N and 145°E at 18 UTC on 24–25 October 2018 (Figure 2(a1,a2)), although the increase in $Chla^{HIMA}$ was not clearer than that at 18°N and 125°E–140°E as shown in Figure 2(a4–a7). This is because the background Chla around 15°N and 145°E is smaller than that at 18°N and 125°E–140°E, where the background Chla is retrieved as follows. For example, the center of the typhoon on October 27 was at 18.0°N and 133.3°E (Figure 2(a4)). The background Chla at the typhoon on October 27 was assumed to be Chla in the same area (18.0°N and 133.3°E) on October 24. The background Chla without cloud disturbance can be retrieve because Figure 2(a1) shows there was no cloud around 18.0°N and 133.3°E on October 24.

The Chla background and R^{HIMA}_{Chla} are the greatest on 30 October, namely 0.18 mg m^{-3} and 8.4, respectively, near the coast of the Philippines along the track of Typhoon Yutu.

The wind speed dependence of R^{HIMA}_{Chla}, R^{MODIS}_{Chla}, δSST^{HIMA} and δSST^{AMSR2} is analyzed using the daily data set of R^{HIMA}_{Chla}, R^{MODIS}_{Chla}, δSST^{HIMA}, δSST^{AMSR2}, longitude and latitude of the center of a typhoon, and the wind speed of a typhoon. Figure 3 shows the wind speed dependence of day 1 (i.e., one day after typhoon arrival) for all typhoons. The numbers of data for R^{HIMA}_{Chla}, R^{MODIS}_{Chla}, δSST^{HIMA}, and δSST^{AMSR2} are 434, 50, 178, and 175, respectively.

Figure 3a shows that R^{HIMA}_{Chla} is proportional to wind speed, namely 0.010 mg m^{-3} $knot^{-1}$ (0.019 mg s m^{-4}), up to approximately 85 knots (44 m s^{-1}). R^{MODIS}_{Chla} is also greater than 1, but the relationship between wind speed and R^{MODIS}_{Chla} is not smooth, e.g., R^{MODIS}_{Chla} has a gap at a wind speed of 60 knots (31 m s^{-1}) because of the small number of data. Stronger wind speed (above 85 knots, 44 m s^{-1}) also increases Chla, but it is likely to have less dependence on wind speed. This is consistent with the work of Lin [6], who showed that the super-typhoon Maemi (whose maximum 10-min sustained wind speed was estimated to be 105 knots (54 m s^{-1}) by the JMA) did not increase Chla. Five outliners of R^{HIMA}_{Chla} were greater than 10; their weekly-averaged Chla may be observed by using polar-orbiting satellites.

Figure 3c,d show δSST^{HIMA} and δSST^{MODIS} on day 1. The decrease in SST^{AMSR2} seems to be also proportional to wind speed up to 85 knots (44 m s^{-1}), whereas that of SST^{HIMA} does not depend on wind speed. δSST^{AMSR2} seems to be also independent of wind speed above 85 knots (44 m s^{-1}).

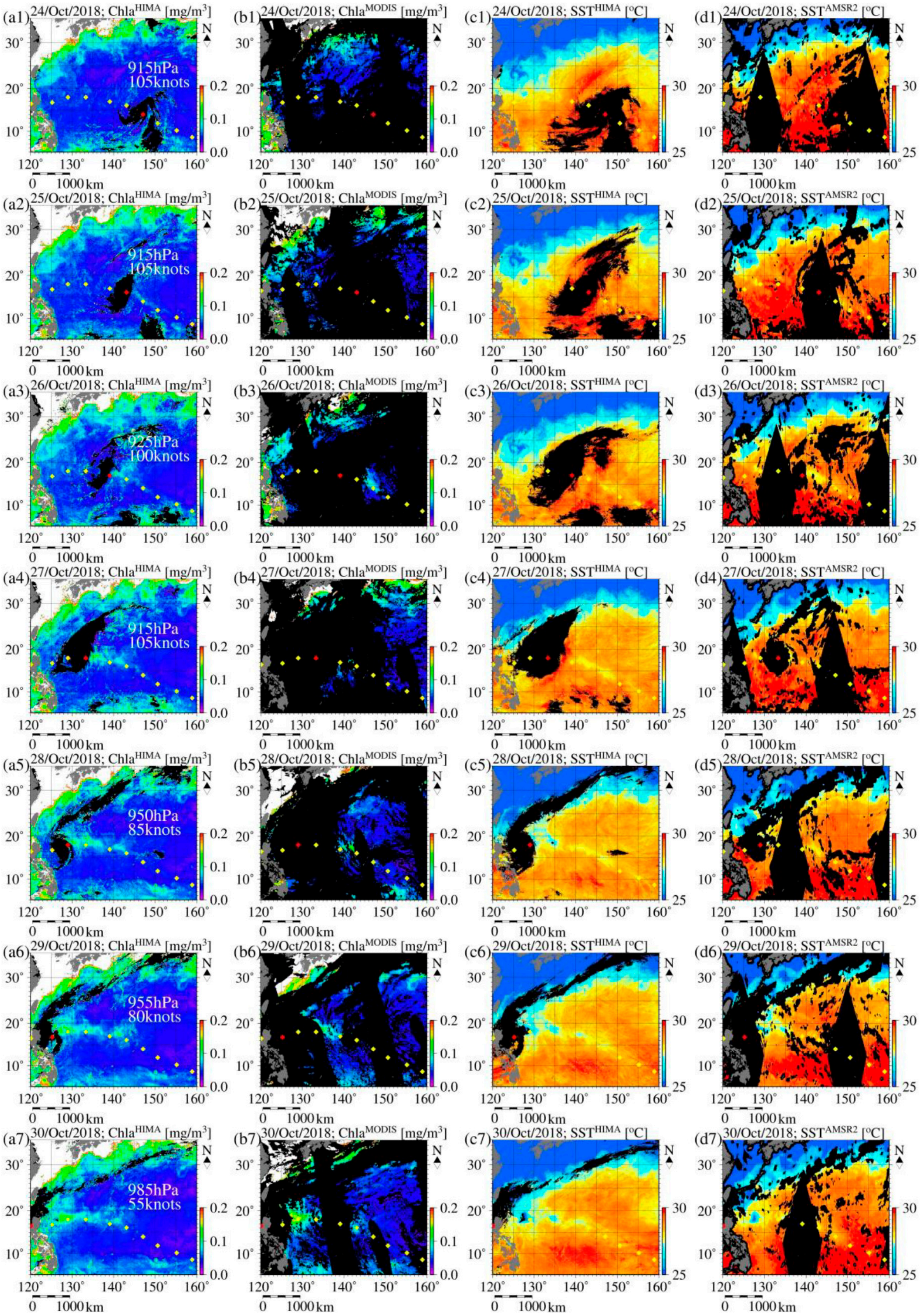

Figure 2. Examples of distributions of Chla^{HIMA} (column **a**), Chla^{MODIS} (column **b**), SST^{HIMA} (column **c**), and SST^{AMSR2} (column **d**) of Typhoon Yutu on 24–30 October 2018. The values of pressure and wind speed were provided in each figure of column a. Black areas denote no data owing to clouds, lack of data, or no ground coverage of the satellite tracks. Gray ones denote no data owing to land. The yellow and red diamonds denote the positions of the center of Yutu at 6 UTC through its lifetime and at the date, respectively. The enlarged figure can be downloaded from the Supplement. (see Figure S1).

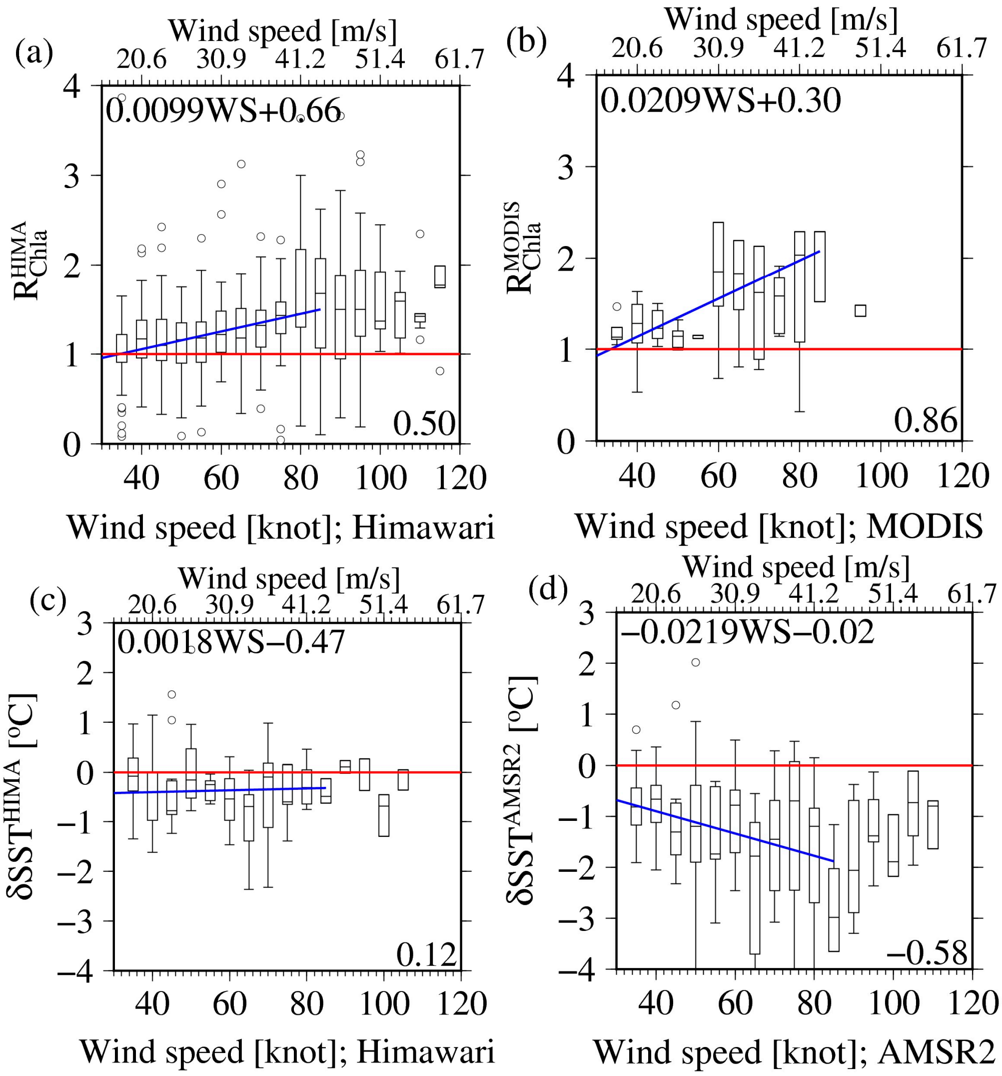

Figure 3. Wind speed dependence of (**a**) R_{Chla}^{HIMA} and (**b**) R_{Chla}^{MODIS}, (**c**) δSST^{HIMA}, and (**d**) δSST^{AMSR2} at day 1, one day after typhoon arrival. All typhoons in all sea areas are considered. Chla (resp. SST) was increased (resp. decreased) when R_{Chla} was greater than 1 (resp. δSST was less than 0) after a typhoon passed. Those thresholds are drawn as red lines. The lowest and highest sides of the rectangles denote the lower quartile (25th percentile, Q1) and upper quartile (75th percentile, Q3), respectively. The horizontal bars in the rectangles denote median (50th percentile). The minimum and maximum bars denote Q1−1.5×IQR and Q3+1.5×IQR, respectively, where IQR denotes Q3−Q1. The white dots denote outliers. Equations and numbers of each figure denote the regression lines and correlation coefficients, respectively, between 35 and 85 knots (between 18 and 44 m s^{-1}), where both are calculated by using the medians of R_{Chla} and δSST at each wind speed to avoid the effect of outliers. WS denotes the wind speed in the unit of knot.

Figure 4 shows the correlation coefficients between wind speed and R_{Chla}^{HIMA} up to 85 knots (54 m s^{-1}) and background $Chla^{HIMA}$. The data are averaged for 100 km from the center of 20°N and 110°E–160°E. The correlation coefficients are around 0.8 at 130°E–160°E, while those in the west from 130°E, such as in the South China Sea and around coastal areas, are around 0.4. This suggests that the Chla increase does not depend clearly on the wind speed in seas with higher Chla.

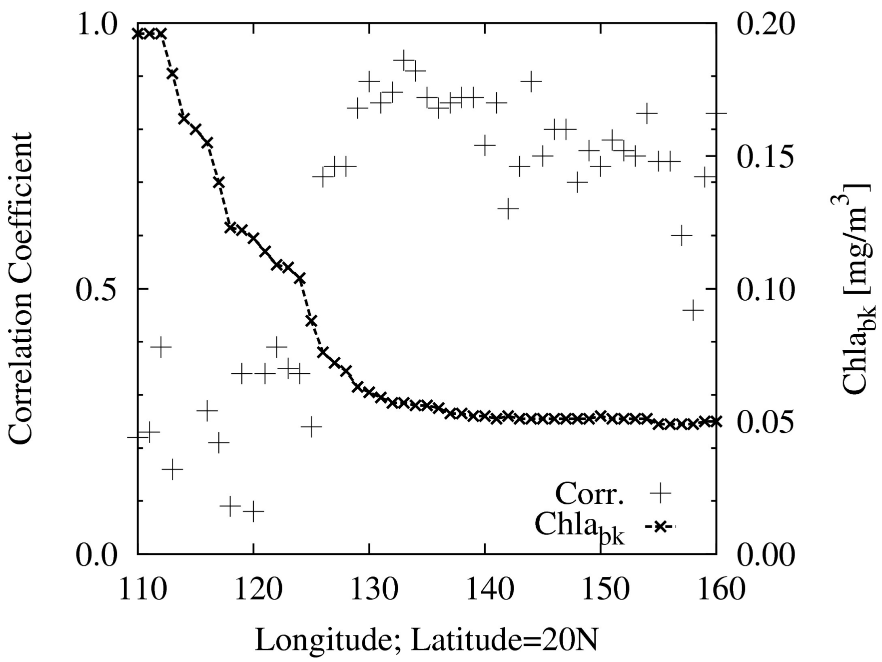

Figure 4. Correlation coefficient between wind speed and R^{HIMA}_{Chla} up to 85 knots (54 m s^{-1}) at day 1 and background levels of Chla^{HIMA}, the Chla^{HIMA} three days before typhoon arrival, Chla$^{HIMA}_{bk}$. The data were averaged for 100 km from the center of 20°N and 110°E–160°E. All correlation coefficients became positive.

Figure 5 shows the tangents of the regression lines for R^{HIMA}_{Chla}, R^{MODIS}_{Chla}, δSST^{HIMA}, and δSST^{AMSR2} from day 0 to 14. Figure 5a shows that R^{HIMA}_{Chla} and R^{MODIS}_{Chla} have the same tendency, but R^{MODIS}_{Chla} is not smooth because of small sample numbers. R^{MODIS}_{Chla} and δSST^{AMSR2} are not calculated for day 0 because of lack of data. The increase in Chla appeared just after day 0 and disappeared within two weeks.

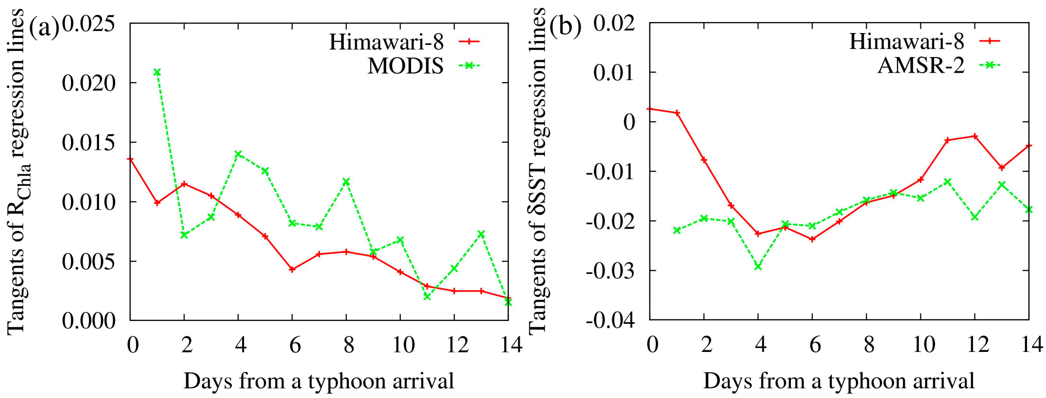

Figure 5. Temporal variations of tangents of regression lines for (**a**) R^{HIMA}_{Chla} and R^{MODIS}_{Chla} and (**b**) δSST^{HIMA} and δSST^{AMSR2} from day 0 to 14. There are no R^{MODIS}_{Chla} or δSST^{AMSR2} calculations at day 0 because of lack of observations, cloudiness, and rainfall.

Donlon et al. [15] showed that the difference between skin SST and bulk SST is around 0.17 °C when the wind speed is greater than 6 m s^{-1}. SST^{HIMA} and SST^{AMSR2} should be the same just after a typhoon has passed. However, as shown in Figure 3c,d, SST^{HIMA} is higher than SST^{AMSR2} at days 1 and 2. SST^{HIMA} starts to decrease from day 0. SST^{HIMA} reaches its minimum after six days from the typhoon's arrival. Both decreases in SST also disappeared within two weeks.

Figures 3d and 5b show that SST^{AMSR2} decreases just after typhoon arrival. This is consistent with the results that R^{HIMA}_{Chla} and R^{MODIS}_{Chla} are the largest just after typhoon arrival (Figure 5a). In general, the amount of nutrients at the sea surface is smaller than that of below the thermocline because phytoplankton uses nutrients in the euphotic zone [16,17]. The increased Chla suggests that the sea surface water is transported from deeper (and colder) water, which contains more nutrients. However, the results indicating that the SST^{HIMA} is not decreased just after typhoon arrival (Figures 3c and 5b) are inconsistent with the above results. Thus, SST^{HIMA} may have a warmer bias at days 0–4, possibly caused by different weather conditions. Namely, the SST^{HIMA} is retrieved only on clear days, whereas the SST^{AMSR2} is retrieved on clear and cloudy days. The cloudier the weather, the larger the difference between SST^{HIMA} and SST^{AMSR2}. This difference should be examined in the future.

4. Conclusions

This study retrieved the empirical characteristics of Chla increase and SST decrease by using the daily Chla and SST products of Himawari-8 for 103 typhoons. The striping noise of the daily Chla of Himawari-8 was removed by using the monthly Chla of Himawari-8 and MODIS. Because the temporal resolution of Himawari-8 is greater than that of polar-orbiting satellites, the Chla and SST retrieved by Himawari-8 are clearer than those due to compositing cloud-free data. That is, the horizontal distribution of the daily $Chla^{HIMA}$ (SST^{HIMA}) showed clearly that $Chla^{HIMA}$ (resp. SST^{HIMA}) was increased (resp. decreased) along the typhoon path after the arrival of a typhoon.

The rate of increase in Chla retrieved by Himawari-8, namely R^{HIMA}_{Chla}, was enhanced when the wind speed of the typhoon became stronger. R^{HIMA}_{Chla} was approximately proportional to wind speed up to approximately 85 knots (44 m s^{-1}), namely 0.010 mg m^{-3} $knot^{-1}$ (0.019 mg s m^{-4}). This relationship was unclear for the $Chla^{MODIS}$ because of fewer data. Chla was the largest at day 0, the day of typhoon arrival, and the increase in Chla disappeared within two weeks. There was likely to be no clear proportional expression between R^{HIMA}_{Chla} and wind speed above 85 knots (54 m s^{-1}), although stronger wind would induce more upwelling. This may be consistent with a previous study of the super-typhoon Maemi, which did not increase the weekly-averaged Chla. Chla is usually increased by a typhoon, but mostly, R^{HIMA}_{Chla} is less than 2. Only a few typhoons appreciably increase Chla.

The decrease in SST^{HIMA} was little and not proportional to wind speed within a few days from typhoon arrival. However, SST^{AMSR2} was the coldest just after typhoon arrival. SST^{HIMA} would have clear-sky bias because SST^{HIMA} was retrieved only on clear days whereas SST^{AMSR2} was retrieved on both clear and cloudy days. SST^{AMSR2} was also proportional to wind speed up to 85 knots (54 m s^{-1}). There is also no clear proportional relation between SST^{AMSR2} and wind speed over 85 knots (54 m s^{-1}).

The above findings were not retrieved by previous polar-orbiting satellites and geostationary satellites. The next step of this work is to estimate the carbon flux by usual typhoons and super-typhoons, which will occur more often in the near future [18].

Supplementary Materials: The following is available online at http://www.mdpi.com/2072-4292/12/8/1259/s1, Figure S1: The enlarged figure of Figure 2.

Author Contributions: S.I. conducted all research work to obtain the results and analyze the data. The author has read and agreed to the published version of the manuscript

Funding: This research received no external funding.

Acknowledgments: Research products of Level 3 of daily and monthly Chla and Level 3 of daily SST of Himawari-8 that were used in this study were supplied by the P-Tree System (https://www.eorc.jaxa.jp/ptree/index.html), Japan Aerospace Exploration Agency (JAXA). Level 3 of daily SST retrieved by AMSR-2 were supplied by the G-Portal System, JAXA (https://gportal.jaxa.jp/gpr/). Level 3 of daily and monthly Chla of MODIS on board the Aqua satellite was provided by the Ocean Biology Processing Group of the Ocean Ecology Laboratory of the NASA Goddard Space Flight Center (https://oceancolor.gsfc.nasa.gov/l3/). The typhoon parameters were provided by the Regional Specialized Meteorological Center, Tokyo (https://www.jma.go.jp/jma/jma-eng/jma-center/rsmc-hp-pub-eg/RSMC_HP.htm). R. Yamashita helped with part of this study.

Conflicts of Interest: The author declares no conflict of interest.

Appendix A. Removal of Noise from Himawari-8 Chla

The Chla product of Himawari-8 contains two types of noise. One is a spikelike noise, although it is not remarkable, and the other is a striping noise [19]. Figure A1a shows the horizontal distribution of monthly Chla without any noise subtractions. The monthly Chla of Himawari-8 looks discrete about every 5° in latitude. The daily Chla also has a striping noise, although it is not noticeable because the variation of the daily Chla is more significant than the striping noise.

I began by using a median filter to reduce the spikelike noise. The median filter converts the value of a certain pixel into the median of nine pixels. That is, a pixel of interest as the center and the eight circumference pixel values are sorted in order of magnitude, and their median value is selected as the value of the pixel of interest.

I then calculated the regression lines between the monthly Chla of Himawari-8 and those of MODIS between August 2015 and October 2019 at each pixel. Because the monthly Chla of MODIS has no striping noise (Figure A1b), I fit the monthly Chla of Himawari-8 to that of MODIS by using the regression lines at each pixel. Figure A1c shows the monthly Chla of Himawari-8 without striping noise. The destriping noise of the daily Chla of Himawari-8 was also removed by using the same regression lines.

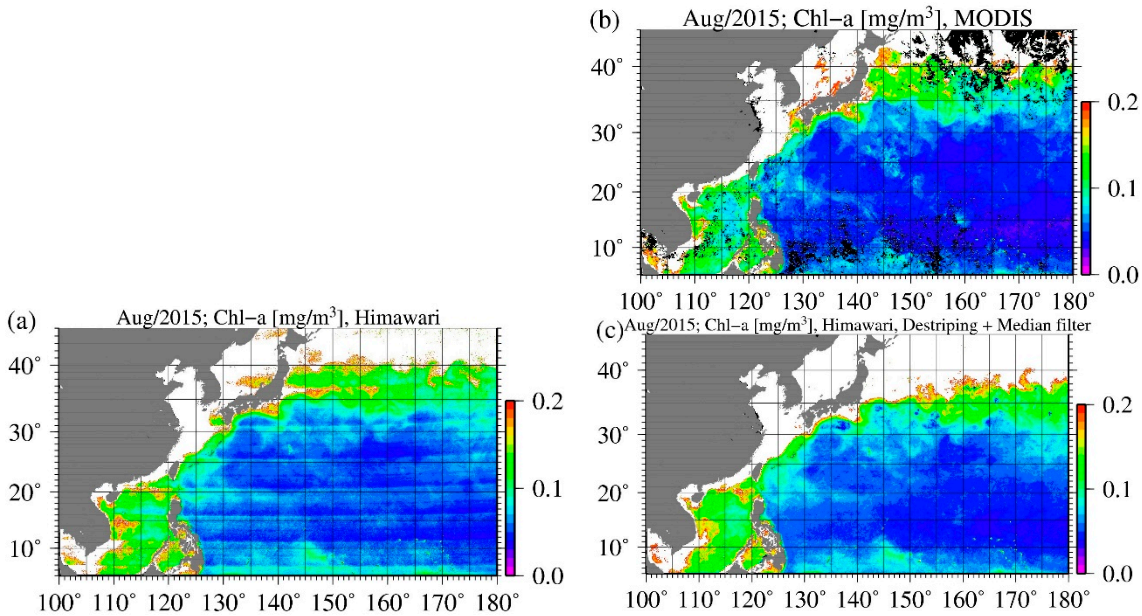

Figure A1. (**a**) Monthly-mean Chla of Himawari on August 2015. (**b**) Same as (**a**) but for MODIS. The black and gray areas denote no data due to cloud and land, respectively. Note that Chla in some areas is not retrieved even for one-month composite data because of sparse temporal resolution. (**c**) Same as (**a**) but with noise removed by median filter and destriping procedure.

References

1. Matsumoto, K.; Honda, M.C.; Sasaoka, K.; Wakita, M.; Kawakami, H.; Watanabe, S. Seasonal variability of primary production and phytoplankton biomass in the western Pacific subarctic gyre: Control by light availability within the mixed layer. *J. Geophys. Res. Ocean.* **2014**, *119*, 6523–6534. [CrossRef]
2. Sun, Y.; Frankenberg, C.; Wood, J.D.; Schimel, D.S.; Jung, M.; Guanter, L.; Drewry, D.; Verma, M.; Porcar-Castell, A.; Griffis, T.J.; et al. OCO-2 advances photosynthesis observation from space via solar-induced chlorophyll fluorescence. *Science* **2017**, *358*, eaam5747. [CrossRef] [PubMed]
3. Shih, Y.-Y.; Hsieh, J.-S.; Gong, G.-C.; Hung, C.-C.; Chou, W.-C.; Lee, M.-A.; Chen, K.-S.; Chen, M.-H.; Wu, C.-R. Field Observations of Changes in SST, Chlorophyll and POC Flux in the Southern East China Sea Before and After the Passage of Typhoon Jangmi. *Terr. Atmos. Ocean. Sci.* **2013**, *24*, 899. [CrossRef]

4. Lin, I.-I.; Wu, C.-C.; Liang, W.; Yang, Y.; Liu, K.-K.; Wong, G.T.F.; Hu, C.; Chen, Z. New evidence for enhanced ocean primary production triggered by tropical cyclone. *Geophys. Res. Lett.* **2003**, *30*, 1718. [CrossRef]
5. Chen, Y.; Tang, D. Eddy-feature phytoplankton bloom induced by a tropical cyclone in the South China Sea. *Int. J. Remote. Sens.* **2012**, *33*, 7444–7457. [CrossRef]
6. Lin, I.-I. Typhoon-induced phytoplankton blooms and primary productivity increase in the western North Pacific subtropical ocean. *J. Geophys. Res. Space Phys.* **2012**, *117*, C3. [CrossRef]
7. Ryu, J.-H.; Han, H.-J.; Cho, S.; Park, Y.-J.; Ahn, Y.-H. Overview of geostationary ocean color imager (GOCI) and GOCI data processing system (GDPS). *Ocean Sci. J.* **2012**, *47*, 223–233. [CrossRef]
8. He, X.; Bai, Y.; Pan, D.; Huang, N.; Dong, X.; Chen, J.; Chen, C.-T.A.; Cui, Q. Using geostationary satellite ocean color data to map the diurnal dynamics of suspended particulate matter in coastal waters. *Remote. Sens. Environ.* **2013**, *133*, 225–239. [CrossRef]
9. Bessho, K.; Date, K.; Hayashi, M.; Ikeda, A.; Imai, T.; Inoue, H.; Kumagai, Y.; Miyakawa, T.; Murata, H.; Ohno, T.; et al. An Introduction to Himawari-8/9–Japan's New-Generation Geostationary Meteorological Satellites. *J. Meteorol. Soc. Jpn.* **2016**, *94*, 151–183. [CrossRef]
10. Shen, D.; Li, X.; Pietrafesa, L.; Bao, S. Geostationary satellite observations and numerical simulation of typhoon-induced upwelling to the Northeast of Taiwan. In Proceedings of the 2017 IEEE International Geoscience and Remote Sensing Symposium (IGARSS), Fort Worth, TX, USA, 23–28 July 2017; pp. 3552–3555. [CrossRef]
11. Japan Aerospace Exploration Agency (JAXA). *GCOM-W1 "SHIZUKU" Data Users Handbook, 2013, Rep. SGC-120011.*; Japan Aerospace Exploration Agency (JAXA): Tokyo, Japan, 2013.
12. Murakami, H. Ocean color estimation by Himawari-8/AHI. In *Remote Sensing of the Oceans and Inland Waters: Techniques, Applications, and Challenges*; International Society for Optics and Photonics: Washington, DC, USA, 2016; Volume 9878, p. 987810. [CrossRef]
13. Carder, K.L.; Chen, F.R.; Lee, Z.; Hawes, S.K.; Cannizzaro, J.P. MODIS Ocean science team algorithm theoretical basis document: Case 2 Chlorophyll. *ATBD* **2003**, *7*, 67.
14. Kurihara, Y.; Murakami, H.; Kachi, M. Sea surface temperature from the new Japanese geostationary meteorological Himawari-8 satellite. *Geophys. Res. Lett.* **2016**, *43*, 1234–1240. [CrossRef]
15. Donlon, C.J.; Minnett, P.J.; Gentemann, C.; Nightingale, T.J.; Barton, I.J.; Ward, B.; Murray, M.J. Toward improved validation of satellite sea surface skin temperature measurements for climate research. *J. Clim.* **2002**, *15*, 353–369. [CrossRef]
16. Open University. *Ocean Circulation, Butterworth Heinemann*; Open University: Milton Keynes, UK, 2001; 286p.
17. Sarmiento, J.L. *Ocean Biogeochemical Dynamics. Ocean Biogeochemical Dynamics*; Princeton University Press: Princeton, NJ, USA, 2006; 528p.
18. Tsuboki, K.; Yoshioka, M.K.; Shinoda, T.; Kato, M.; Kanada, S.; Kitoh, A. Future increase of supertyphoon intensity associated with climate change. *Geophys. Res. Lett.* **2015**, *42*, 646–652. [CrossRef]
19. Weinreb, M.; Xie, R.; Lienesch, J.; Crosby, D. Destriping GOES images by matching empirical distribution functions. *Remote. Sens. Environ.* **1989**, *29*, 185–195. [CrossRef]